Article

Journal of Orthopaedic Surgery

Journal of Orthopaedic Surgery
26(3) 1–10

DOI: 10.1177/2309499018802487
journals.sagepub.com/home/osj
SAGE

Bisphosphonates reduce biomaterial turnover in healing of critical-size rat femoral defects

Michel Hauser[1,2], Mark Siegrist[1], Alain Denzer[1], Nikola Saulacic[3], Joël Grosjean[4], Marc Bohner[5] and Willy Hofstetter[1]

Abstract

Treatment of osteoporotic patients with bisphosphonates (BPs) preserves bone mass and microarchitecture. The high prescription rate of the drugs brings about increases in the numbers of fractures and bone defects requiring surgical interventions in these patients. Currently, critical-size defects are filled with biomaterials and healing is supported with bone morphogenetic proteins (BMP). It is hypothesized that BPs interfere with biomaterial turnover during BMP-supported repair of defects filled with β-tricalcium phosphate (βTCP) ceramics. To test this hypothesis, retired breeder rats were ovariectomized (*OVX*). After 8 weeks, treatment with alendronate (ALN) commenced. Five weeks later, 6 mm diaphyseal femoral defects were applied and stabilized with locking plates. βTCP cylinders loaded with 1 μg and 10 μg BMP2, 10 μg L51P, an inhibitor of BMP antagonists and 1 μg BMP2/10 μg L51P were fitted into the defects. Femora were collected 16 weeks post-implantation. In groups receiving calcium phosphate implants loaded with 10 μg BMP2 and 1 μg BMP2/10 μg L51P, the volume of bone was increased and βTCP was decreased compared to groups receiving implants with 1 μg BMP2 and 10 μg L51P. Treatment of animals with ALN caused a decrease in βTCP turnover. The results corroborate the synergistic effects of BMP2 and L51P on bone augmentation. Administration of ALN caused a reduction in implant turnover, demonstrating the dependence of βTCP removal on osteoclast activity, rather than on chemical solubility. Based on these data, it is suggested that in patients treated with BPs, healing of biomaterial-filled bone defects may be impaired because of the failure to remove the implant and its replacement by authentic bone.

Keywords

bisphosphonate, BMP2, fracture healing, osteoporosis, β-tricalcium phosphate

Date received: 30 May 2018; accepted: 2 September 2018

Introduction

Each year, worldwide more than 8.9 million osteoporosis-related fractures are counted.[1] Loss of bone mass and deterioration of microarchitecture in post-menopausal women are the primary causes for the increase in fracture risk. Bisphosphonates (BPs) are widely considered as the drugs of choice for the prevention of bone loss in post-menopausal osteoporosis. BP bind to calcium phosphate (CaP) minerals with high and prolonged affinity.[2,3] Upon cellular uptake, the drugs block osteoclastic bone resorption, resulting in stabilization of bone mass and preservation of structure.[2,3] Administration of alendronate (ALN),

[1] Bone Biology & Orthopaedic Research, Department for BioMedical Research (DBMR), University of Bern, Bern, Switzerland
[2] Graduate School for Cellular and Biomedical Sciences, University of Bern, Bern, Switzerland
[3] Clinic for Cranio-Maxillofacial Surgery, Department for BioMedical Research (DBMR), University of Bern, Bern, Switzerland
[4] Urology Research Group, Department for BioMedical Research (DBMR), University of Bern, Bern, Switzerland
[5] RMS-Foundation, Bettlach, Switzerland

Corresponding author:
Willy Hofstetter, Bone Biology & Orthopaedic Research, Department for BioMedical Research (DBMR), University of Bern, Murtenstrasse 35, 3008 Bern, Switzerland.
Email: hofstetter@dbmr.unibe.ch

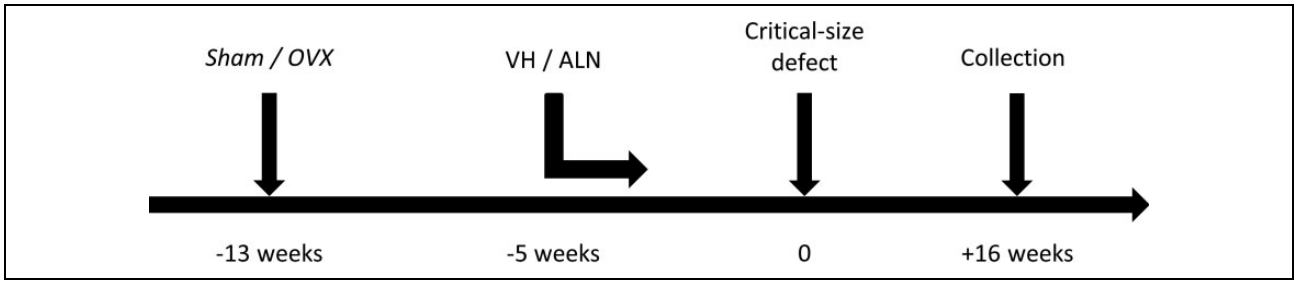

Figure 1. Time course/experimental design of ALN-treated osteoporotic femoral defect model. Thirteen weeks before the femoral critical-size defect, animals were either *OVX* or *sham*-operated. VH or ALN (in *OVX* only) was administered twice a week s.c. 5 weeks prior to insertion of the femoral defect until sacrifice. Mid-diaphysis femoral defects (6 mm) were stabilized with a PEEK plate with six interlocking screws (RatFix™, RISystem), and a βTCP cylinder was placed within the defect. Samples were collected 16 weeks after femoral surgery for histological analysis and microCT measurements. VH: vehicle; PEEK: polyether ether ketone; ALN: alendronate; *OVX*: ovariectomized; βTCP: β-tricalcium phosphate; microCT: micro-computer tomography.

the most frequently prescribed BP, results in a reduction of hip and vertebral fractures.[4–9] Because BPs are widely used and elderly patients with osteoporosis are prone to fractures, there has been an interest to understand the effects of BP on bone repair. In vivo studies on fracture healing in rodents reported an increase in callus size and a delay in bone remodelling upon treatment with ALN.[10–12] Furthermore, in a number of surgical interventions such as spinal fusion or the repair of large bone defects, bone morphogenetic proteins (BMP), such as BMP2 and BMP7, and CaP-based biomaterials need to be used. To achieve clinical efficacy, however, these growth factors are administered in supraphysiological dosages.[13] This may be caused, at least in part, by a reduction in bioavailability of the BMP, since the growth factors induce the expression of antagonists at the repair site.[14,15] Indeed, an increase in the expression of BMP antagonists was demonstrated during fracture healing and distraction osteogenesis.[16–18] Furthermore, biomaterials need to be removed in a timely manner to allow for efficient replacement by authentic bone. To this purpose, it is essential to ensure that implant removal is governed by cellular processes rather than solely chemical dissolution. To improve the bioavailability of BMP2, L51P, an in vitro engineered BMP2 variant with a leucine to proline substitution at amino acid 51, was developed. This modified protein does not activate BMP type I receptor but has affinity for BMP type II receptors and the BMP antagonists noggin, gremlin and others.[19] After demonstrating that L51P restored BMP2-mediated osteoblast differentiation by inhibiting noggin in vitro,[20] we and others reported that L51P increased the biological efficacy of BMP2 and that the amount of BMP2 required to induce clinically relevant bone formation in a femoral critical-size segmental defect rat model[21] or in a calvaria defect model[22,23] could be reduced. Since BP were shown to stabilize bone mass and to maintain bone microarchitecture by reducing osteoclastic resorption and total bone turnover, the administration of BP, in the presence of bioavailable BMP2, has been hypothesized to possibly lead to impaired bone healing. The aim of the present study was to evaluate the effects of ALN on the healing process of a critical-size defect, filled with CaP ceramics, in the femora of osteoporotic rats in the presence of BMP2 and L51P. The data suggest that healing is impaired by ALN due to the attenuated turnover of the biomaterial.

Methods

Experimental design

This study was approved by the local committee for animal experimentation (Bern Committee for the Control of Animal Experimentation, Bern, Switzerland, permit number BE67/16 to WH). Wistar Crl: WI (Han) rats (female, retired breeders, 8–10 months old and weighing 285–580 g) were purchased from Charles River (Sulzfeld, Germany). The animals were housed in the Central Animal Facility of the Medical Faculty, University of Bern, Switzerland, in compliance with the Swiss Federal Government guidelines for care and use of experimental animals. Animals were allocated to one of three groups (*sham,* ovariectomized (*OVX*)/vehicle and *OVX*/ALN) based on their bodyweight such that the average weight of the animals was not statistically different among the groups. For this purpose, the animals, after equilibration in the facility and before *OVX*, were divided into three groups (high, medium and low weight) and the animals from each weight group were randomly allocated to each experimental group using a Random Number Generator for iPad. The experimental design and the time course of the study are depicted in Figure 1. Briefly, at $t = 0$, animals were either *OVX* or *sham*-operated. ALN (*OVX* only) or vehicle (*sham/OVX*) treatment was initiated 8 weeks after *OVX* and continued until sacrifice. A critical-size defect was applied in the left femur 5 weeks after the onset of vehicle/ALN treatment (13 weeks post-*OVX*) and stabilized with a rigid osteosynthesis system (RatFix™, RISystem AG, Davos, Switzerland). For all surgical procedures, the rats were anaesthetized by subcutaneous injections (1 ml/kg body weight) of a 1:2 mixture

of ketamine hydrochloride (33 mg/kg body weight; 100 mg/ml) and xylazine hydrochloride (13.3 mg/kg body weight; 20 mg/ml). During surgery, the animals were placed on a heating pad to prevent hypothermia. Group sizes were $n = 6$. Sixteen weeks after femoral surgery, euthanization of animals was performed using CO_2, followed by cervical translocation, and samples were collected for micro-computer tomography (microCT) and histological analysis. In total, 12 experimental groups were used, encompassing a total of 72 rats.

Ovariectomy

After shaving and disinfection, the ovaries were approached through two 2.5 cm flank incisions at the mid-dorsum. The skin was detached from the underlying muscles before incising the muscles. The ovaries were identified, clamped and removed (gently pulled through the incisions and a haemostat was placed between the oviduct and the ovaries). The oviducts were ligated and a cut was made between the haemostat and the ovaries. Haemostasis was controlled before replacing the ligated oviducts in the abdomen. The muscle layer was closed with absorbable sutures, and the skin was sutured with non-absorbable thread. *Sham*-operated animals underwent the same surgical procedures, except for the ligation of the oviducts and the removal of the ovaries.

BP treatment

ALN solution was prepared as previously described[24] and dissolved in 0.9% NaCl. ALN (1.61 µmol/kg body weight; 2 ml/kg bodyweight) or vehicle (0.9% NaCl solution; 2 ml/kg body weight) was subcutaneously injected 8 weeks after *OVX* twice weekly until sacrifice. After 8 weeks, bone mass was significantly reduced in *OVX* animals as compared to *sham* controls.

Loading of ceramic β-tricalcium phosphate cylinders with peptides and release kinetics

Ceramic β-tricalcium phosphate (βTCP) cylinders (diameter 5 mm, length 6 mm and porosity 75%) were used as described previously[21] and were generously provided by the Robert Mathys Foundation (Bettlach, Switzerland). The BMP2 and L51P proteins were expressed in *Escherichia coli* and were kindly provided by Prof. W Sebald, University of Würzburg, Germany.[19,25,26] For the measurement of the in vitro release of L51P and BMP2 from the ceramics, 1 or 10 µg of BMP2 or L51P was dissolved in 25 µl of deionized water and adsorbed onto βTCP carriers. After 24 h of drying at room temperature, the loaded ceramics were incubated in 1.5 ml culture medium (alpha-minimum essential medium, 10% foetal bovine serum and 1% penicillin/streptomycin) for 16 days. The medium was changed after 24 h, and after 2, 4, 8 and 16 days. The amounts of BMP2 and L51P released into the culture medium were quantified using an ELISA kit for the detection of BMP2 and L51P (Human BMP2 ELISA development kit, Peprotech, Rocky Hill, Connecticut, USA).

Table 1. BMP2 and L51P loading of βTCP carriers.

Experimental groups				
I	II	III	IV	V
Unloaded	1 µg BMP2	10 µg BMP2	10 µg L51P	1 µg BMP2/ 10 µg L51P

βTCP: β-tricalcium phosphate; BMP: bone morphogenetic protein.

Fixation of the critical-size femoral defect and implantation of βTCP cylinders

For the loading of the βTCP implants to fill the critical-size defects, BMP2 and L51P were dissolved in 25 µl of deionized water and adsorbed to βTCP carriers (Table 1). The loaded carriers were air-dried overnight at room temperature and implanted into 6 mm critical-size segmental diaphyseal bone defects in the rat femora (five groups, $n = 6$ per group), as recommended by the manufacturer (https://vimeo.com/130984695). Thirteen weeks after *OVX* and five weeks after the commencement of the ALN treatment, the central part of the left mid-diaphyseal femur (6 mm) was surgically removed. After shaving and disinfection of the skin, a longitudinal incision in line with the left femur was cut on the lateral thigh. The interval between the *vastus lateralis* and the *biceps femoris* was developed to expose the bone, the *gluteus superficialis* tendon was detached from the *trochanter tertius* and the RatFix™ System (RISystem AG, Davos, Switzerland) was mounted onto the intact femora using six interlocking screws. Subsequently, using two Gigli saws, two osteotomies were created between the two central screws, and the central mid-diaphyseal bone fragment was collected for further analysis. Care was taken not to harm the surrounding periosteum. Debris was removed by rinsing the defect site with sterile physiological saline solution. Subsequently, a βTCP implant, which was stabilized with a non-absorbable polypropylene thread, was inserted into the defect and the wound was closed. After the animals recovered from anaesthesia, analgesia was performed for 3 days, using Temgesic (0.0075 mg/kg body weight; 0.3 mg/ml), and full load bearing and unrestricted cage activity were allowed. Movement or instability of the implants and failure of the osteosynthesis were monitored using high-resolution X-ray imaging immediately after surgery. After 16 weeks, the implants, together with the surrounding tissues, were harvested and analysed.

X-ray

After surgery, the integrity of the surgical site was documented using high-resolution radiography, applying the following image acquisition parameters: 25 kV and 10 s acquisition time (MX-20, Faxitron X-Ray Corporation, Edimex, Le Plessis, France). No animals needed to be excluded from the experiment post-operatively because of incorrect defect localization and/or plate positioning.

Peripheral quantitative computed tomography

The effects of *OVX* on bone mass and structure were evaluated using in vivo peripheral quantitative computed tomography (pQCT; XCT Research SA, Stratec Medizintechnik GmbH, Birkenfeld, Germany) measurements at the left distal femur and proximal tibia, 7 weeks after *OVX*, using the following parameters: voxel size, 70 μm; High Voltage, 50 kV; and acquisition time, 10 min. For pQCT analysis, animals were anaesthetized as described above.

Micro-computer tomography

The tissues for histological and microCT analysis were fixed with 4% paraformaldehyde in Phosphate Buffered Saline (PBS) for 24 h, and subsequently transferred to 70% ethanol. Polyether ether ketone (PEEK) plate and Titanium screws remained in situ for these analyses. For microCT analysis (MicroCT40, SCANCO Medical AG, Brüttisellen, Switzerland), the built-in software from SCANCO was used (SCANCO Module 64-bit; V5.15). The long axis of the femur was oriented orthogonally to the axis of the X-ray beam. The X-ray tube was operated at 70 kVp and 114 μA, and the integration time was set at 200 ms. The measurements were performed perpendicular to the longitudinal axis of the femora. Bone growth was evaluated in the area between the two central screws of the fixation systems. To distinguish between soft and mineralized tissues, the tissue was segmented into two tissue types based on their greyscale (grey-level coded mineralization density), that is, <200 Hounsfield unit (HU) for soft tissues and >200 HU for mineralized tissues (βTCP carrier, mineralized cartilaginous callus, woven and lamellar bone).[27] Cortical thickness was measured using the SCANCO built-in algorithm. The analysis was performed with a voxel size of 8 μm.[28]

Histological analysis and histomorphometry

After microCT analysis, the tissues were embedded in methyl methacrylate as described previously.[29] Thereafter, ground sections of approximately 200 μm were prepared (Leica SP1600, Leica Microsystems, Glattbrugg, Switzerland). The sections were polished and stained with McNeal tetrachrome.[30,31] Microphotographs were taken using a Nikon Eclipse E800 microscope (Nikon Inc., Egg, Switzerland). Bone formation and implant turnover were determined by the ImageJ trainable segmentation plugin; Waikato Environment for Knowledge Analysis (WEKA) automated segmentation histomorphometry[32] on 4 serial McNeal tetrachrome-stained ground sections per implant. The sum of the surface area of bone and implant was determined for each animal (four sections/animal). The total bone surface area and implant surface area per treatment group were computed.

Uterus dry weight

Uteri were collected *post-mortem*, stored overnight at room temperature, and the dry weight was measured 24 h after collection.

Statistical analysis

The following statistical analyses were performed using GraphPad Prism 7 for Windows (GraphPad Software, San Diego, California, USA, www.graphpad.com). Unpaired *t*-test was used for bodyweight and uterus dry weight analysis; two-way analysis of variance (ANOVA) with Tukey post hoc was applied to pQCT, microCT and histomorphometry analysis. Mean values with standard deviations are shown. Significant at $p < 0.05$. For multiple testing, $p_{adj} < 0.05$ was considered significant.

Results

Release of BMP2 and L51P from βTCP ceramics

BMP2 and L51P were released in vitro with identical kinetics over the course of 16 days, as determined by ELISA (data not shown).

Bone loss in OVX rats and the effects of BP

The effect of *OVX* on bone mass was determined in vivo by pQCT analysis in proximal tibiae and distal femora at time of *OVX* and 7 weeks thereafter. Cortical and trabecular densities did not vary between *OVX* and *sham* groups at the time of surgery. After 7 weeks, both cortical and trabecular densities were significantly decreased in *OVX* animals in measurements at four different tibial sites (tibia position 1: 1122.4 $\pm$ 49.4 mg/cm^3 vs. 1022.6 $\pm$ 42.3 mg/cm^3, $p < 0.0001$; 248.2 $\pm$ 60 mg/cm^3 vs. 203 $\pm$ 57.3 mg/cm^3, $p = 0.0002$; Figure 2).

To confirm the efficiency of *OVX*, uterine dry weight was measured *post-mortem*. Uterine dry weight was reduced by 40% in *OVX* animals as compared to that in *sham*-operated animals. (*sham* vs. *OVX* + vehicle, 248.4 $\pm$ 62.9 mg vs. 138.7 $\pm$ 41.4 mg, $p = 0.0001$; *sham* vs. *OVX* + ALN, 248.4 $\pm$ 62.9 mg vs. 143.2 $\pm$ 37.3 mg, $p = 0.0001$; Online Supplemental Figure 1).

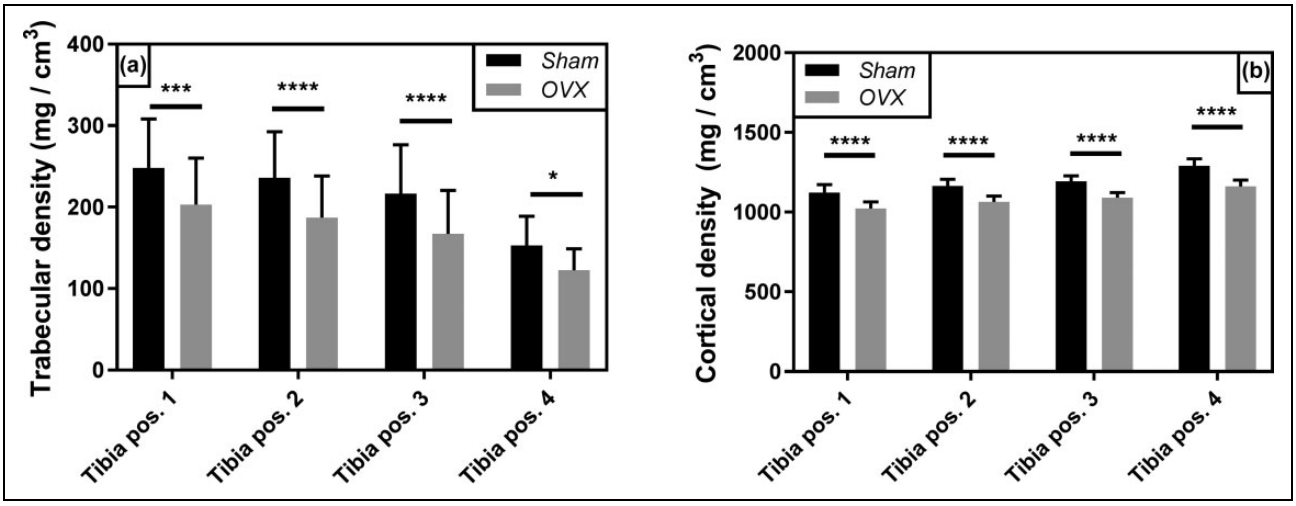

Figure 2. In vivo pQCT measurements of tibial trabecular and cortical densities. Densities of cortical and cancellous bone were measured 7 weeks post-*OVX* by pQCT. (a) Trabecular density of the proximal tibiae. (b) Cortical density of the proximal tibiae. Densities of both trabecular and cortical bones of *OVX* animals significantly decreased as compared to those of *sham* animals in four virtual sections, measured 0.3 mm step from mid-joint (tibia 1–4). Two-way ANOVA with Tukey post hoc, *OVX* vs. *sham* for each time point. *$p < 0.05$, ***$p < 0.001$, ****$p < 0.0001$, $n = 24$. pQCT: peripheral quantitative computed tomography; *OVX*: ovariectomized; ANOVA: analysis of variance.

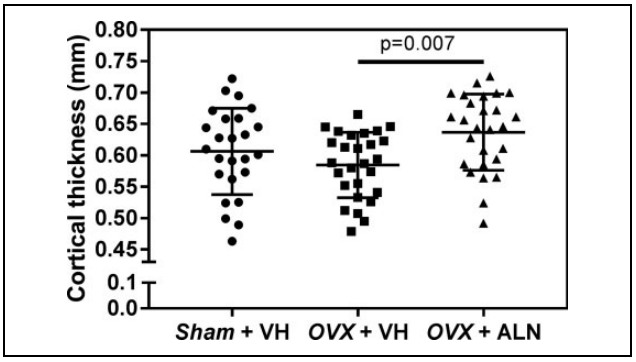

Figure 3. Cortical thickness of femoral diaphysis. Cortical thickness of the femoral mid-diaphysis collected during femoral surgery was assessed by microCT. A significant increase in the cortical thickness was observed in bones from ALN-treated animals as compared to those from vehicle-treated *OVX* rats. Kruskal–Wallis with Dunn's post hoc test, $n = 25$–27. MicroCT: micro-computer tomography; ALN: alendronate.

Treatment with ALN leads to an increase in cortical thickness

To assess the effects of ALN treatment in *OVX* animals, cortical thickness was determined by microCT analysis of the mid-diaphyseal fragments collected during the creation of femoral critical-size defects (corresponding to 13 weeks after *OVX* and 5 weeks after onset of the ALN treatment). Administration of ALN resulted in a significant increase of the cortical thickness as compared to that in vehicle treated *OVX* animals (0.64 $\pm$ 0.06 mm vs. 0.58 $\pm$ 0.05 mm, $p = 0.0066$; Figure 3).

Bone formation is stimulated by BMP2 and implant turnover is reduced by ALN

Sixteen weeks after implantation, no bone formation and osseointegration of the CaP implant was observed in the critical-size defects upon insertion of unloaded βTCP (control) cylinders irrespective of *sham*/*OVX* and vehicle/ALN treatments (Figures 4(a), (f), (k) and 5(a)). Similarly, no bone formation was found when the defects were filled with 10 µg L51P-loaded βTCP cylinders, again independently of the applied treatment protocols (*sham*, 1.55 $\pm$ 0.39 mm^2 (unloaded) and 1.84 $\pm$ 0.31 mm^2 (L51P), $p = 0.9998$; *OVX*/vehicle, 1.37 $\pm$ 0.27 mm^2 and 2.14 $\pm$ 0.81 mm^2, $p = 0.9942$; *OVX*/ALN, 1.87 $\pm$ 0.57 mm^2 and 2.89 $\pm$ 2.14 mm^2, $p = 0.9708$; Figures 4(d), (i), (n) and 5(a)). Some bone formation was detected in defects filled with 1 µg BMP2-loaded βTCP cylinders (Figure 4(b), (g), (l)), but quantitative histomorphometry revealed no significant increase in bone formation as compared to unloaded βTCP cylinders, irrespective of *sham/OVX* and vehicle/ALN treatments (*sham*, 1.55 $\pm$ 0.39 mm^2 vs. 3.12 $\pm$ 2.62 mm^2, $p_{adj} = 0.9272$; *OVX*/vehicle, 1.37 $\pm$ 0.27 mm^2 vs. 4.25 $\pm$ 2.82 mm^2, $p = 0.6185$; *OVX* + ALN, 1.87 $\pm$ 0.57 mm^2 vs. 5.76 $\pm$ 4.24 mm^2, $p = 0.2954$; Figure 5(a)). Induction of bone formation was observed with βTCP cylinders loaded either with 10 µg BMP2 (*sham*, 1.55 $\pm$ 0.39 mm^2 vs. 12.41 $\pm$ 5.02 mm^2, $p = 0.0003$; *OVX*/vehicle, 1.37 $\pm$ 0.27 mm^2 vs. 10.41 $\pm$ 2.37 mm^2, $p = 0.0004$; *OVX*/ALN, 1.87 $\pm$ 0.57 mm^2 vs. 14.49 $\pm$ 4.06 mm^2, $p = 0.0001$; Figures 4(c), (h), (m) and 5(a)) or 1 µg BMP2/10 µg L51P (*sham*, 1.55 $\pm$ 0.39 mm^2 vs. 9.86 $\pm$ 4.51 mm^2, $p = 0.0031$; *OVX*/ALN, 1.87 $\pm$ 0.57 mm^2 vs. 12.62 $\pm$ 5.95 mm^2, $p = 0.0001$; Figures 4(e), (o) and 5(a)). In *OVX*

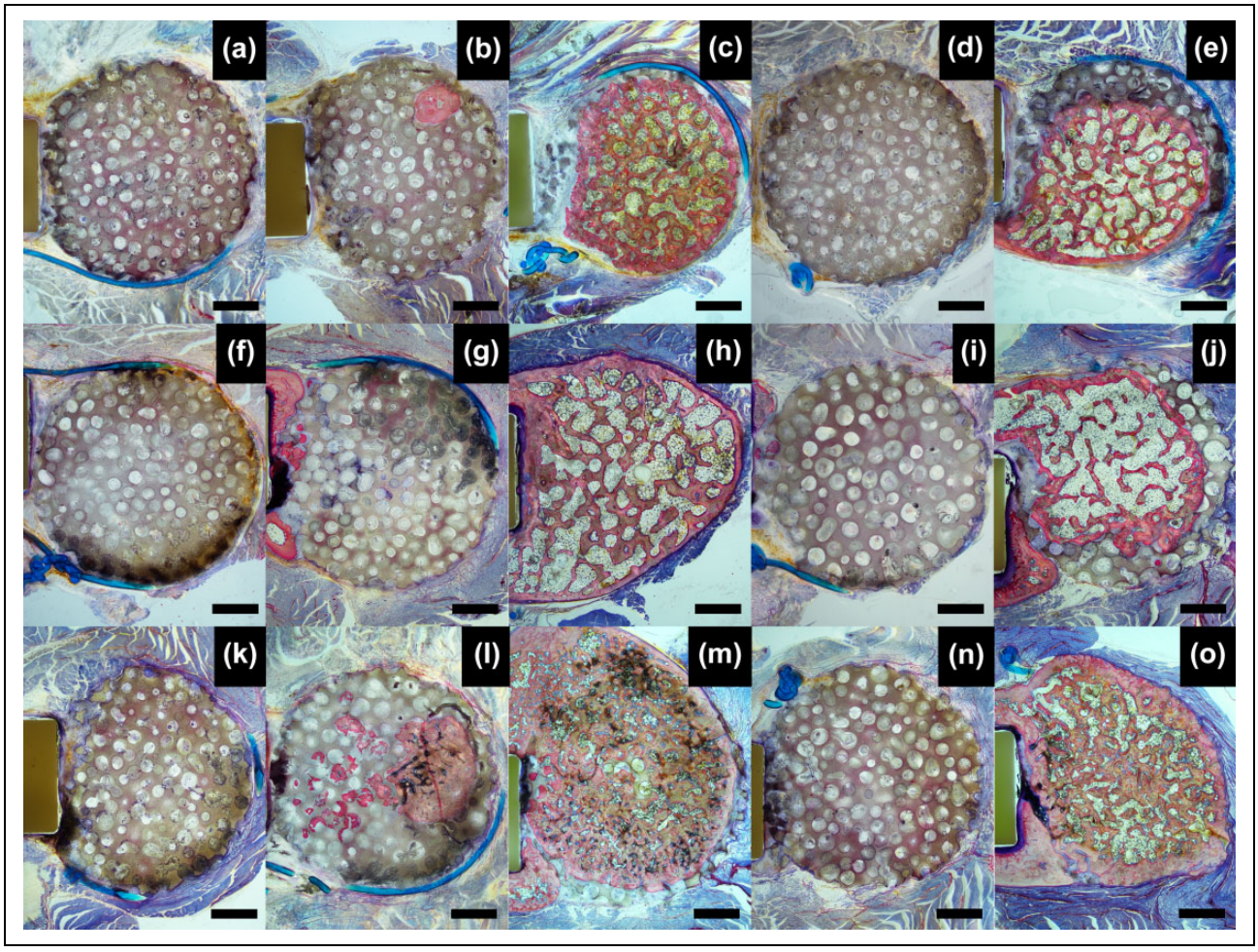

Figure 4. Methyl metacrylate histologies of βTCP ceramics in femoral critical-size defects. Cross sections of βTCP cylinders implanted in critical-size femoral defects collected 16 weeks after surgery and stained with McNeal tetrachrome are shown. Implants from *sham* animals (a–e); implants from vehicle-treated *OVX* rats (f–j); implants from *OVX* animals treated with ALN (k–o). No bone growth was observed in animals that received empty control ceramics (a, f, k) or ceramics loaded with 10 μg L51P (d, i, n) irrespective of *sham*/*OVX* and ALN/vehicle treatments. Little and irregular bone formation was observed in ceramics loaded with 1 μg BMP2 (b, g, l) irrespective of *sham*/*OVX* and ALN/vehicle treatments. Bone formation was observed in animals with implants loaded with 10 μg BMP2 (c, h, m) or 10 μg L51P/1 μg BMP2 (e, j, o) irrespective of *sham*/*OVX* and ALN/vehicle treatments. Increased volumes of residual ceramics were observed in ALN-treated animals with βTCP implants loaded with 10 μg BMP2 (m) and 10 μg L51P/1 μg BMP2 (o) compared to vehicle-treated animals with βTCP implants loaded with 10 μg BMP2 (c, h) or 10 μg L51P/1 μg BMP2 (e, j). Bars represent 1 mm. ALN: alendronate; *OVX*: ovariectomized; βTCP: β-tricalcium phosphate; BMP: bone morphogenetic protein.

animals receiving βTCP cylinders loaded with 1 μg BMP2/10 μg L51P (Figure 4(j)), no significant increase in bone formation was detected (1.37 ± 0.27 mm^2 vs. 5.81 ± 2.84 mm^2, $p = 0.1356$). As previously observed,[21] bone formation was associated with implant turnover in *sham*-operated animals. An increased volume of residual βTCP implant material remained in the defect site in ALN-treated animals as compared to vehicle-treated animals receiving βTCP implants with identical protein loads (10 μg BMP2 (*OVX*/vehicle vs. *OVX*/ALN, 1.99 ± 0.52 mm^2 vs. 5.48 ± 1.62 mm^2, $p_{adj} < 0.0001$; Figures 4(m) and 5(b)); 1 μg BMP2/10 μg L51P (*OVX*/vehicle vs. *OVX*/ALN, 1.39 ± 0.72 mm^2 vs. 4.33 ± 1.20 mm^2, $p_{adj} < 0.0001$; Figures 4(o) and 5(b)). Although minimal extra-implant/peripheral bone formation was observed in vehicle-treated animals whose defects were filled with 10 μg BMP2 and 1 μg BMP2/10 μg L51P loaded βTCP cylinders (Figure 4(c), (e), (h), (J)), respectively, extensive peripheral bone formation was observed in defects from ALN-treated animals (Figure 4(m), 4(o)) with identical βTCP loading conditions. After 16 weeks, microCT renderings of the defect sites revealed that βTCP cylinders loaded with 10 μg BMP2 or 1 μg BMP2/10 μg L51P formed an interface with the host bone. In defects from vehicle-treated animals in which implants were loaded with 10 μg BMP2 or 1 μg BMP2/10 μg L51P, bone formation

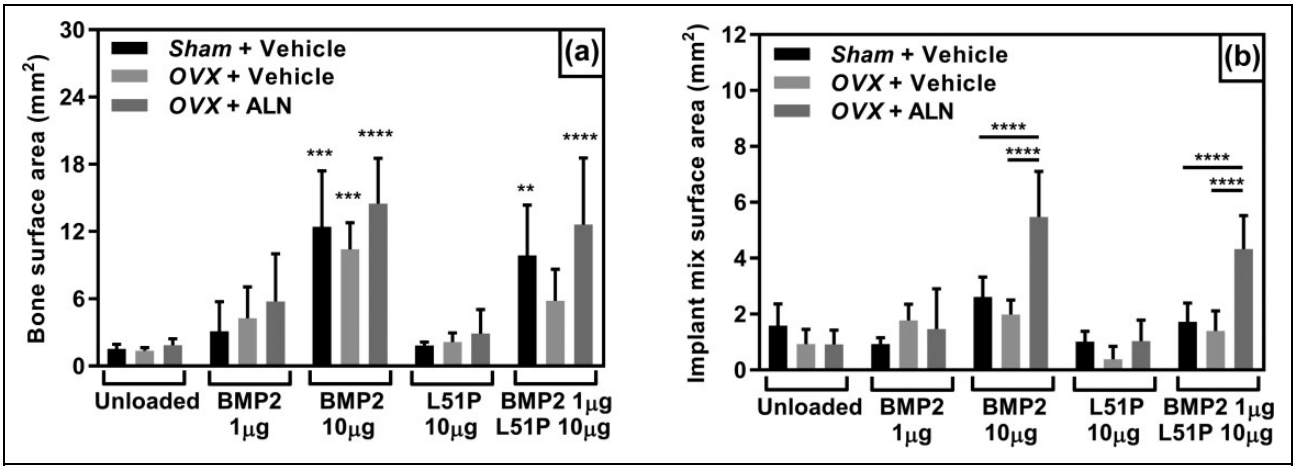

Figure 5. Bone formation and βTCP turnover. Bone formation and turnover of βTCP ceramics were quantified by automated histomorphometry. The surface areas of bone and implant were computed with WEKA (automated segmentation) on four sections per animal. (a) Total bone surface area in treatment groups. Bone formation was significantly increased with 10 μg BMP2, irrespective of *sham*/*OVX* and vehicle/ALN. A significant increase in bone formation was observed in *sham*/ALN and *OVX*/ALN animals with ceramics loaded with 1 μg BMP2/10 μg L51P. (b) Total ceramics surface areas in treatment groups. Residual surface of βTCP ceramics was significantly larger in ALN-treated animals whose defects were filled with implants coated with either 10 μg BMP2 or 1 μg BMP2/10 μg L51P than in *sham* and *OVX* control animals. Two-way ANOVA with Tukey post hoc, compared to treatment protocol (*OVX*/*sham,* VH/ALN) matched unloaded βTCP cylinder. *Significant at $p < 0.05$, ***significant at $p < 0.001$, ****significant at $p < 0.0001$, $n = 3$–6. WEKA: Waikato Environment for Knowledge Analysis; ALN: alendronate; *OVX*: ovariectomized; βTCP: β-tricalcium phosphate; BMP: bone morphogenetic protein.

occurred from either the distal or proximal end of the defect and did not fill the entire implant. In contrast, defects in ALN-treated animals filled with βTCP cylinders loaded with 10 μg BMP2 or 1 μg BMP2/10 μg L51P were characterized by a bone continuum throughout the entire βTCP implant (Figure 6). MicroCT analysis of serial cross-sections along the longitudinal axis of the defects suggested that the surface area of bone was decreasing from the bone–implant interface towards the centre of the implant. Evaluation of cross-sectional 2-D microCT images confirmed the reduction of the bone surface area from the bone–implant interface towards the centre of the defect (Figure 7).

Discussion

BP are the most frequently prescribed drugs to preserve bone mass and microarchitecture. Treatment with BP and the consequential maintenance of the bone substance results in a decrease in the risk to sustain wrist, vertebral and hip fractures in patients suffering from osteoporosis.[4, 7, 9] Because prolonged treatment with BP causes bone turnover to slow down, and because the concept of a drug holiday during BP treatment is controversially discussed,[33] it is an open question whether bone repair is impaired by concurring treatment with BP in osteoporotic patients. The present study aimed to answer several aspects of repair of a critical-size femoral defect, with βTCP as a bone filler, in estrogen deficient osteoporotic rats treated with BP such as (i) the preservation of the previously described synergistic effect of BMP2 and L51P on bone healing, (ii) the effects of BP treatment on bone repair and remodelling of the defect site and (iii) the turnover of a βTCP implant under conditions of blocked osteoclast activity. The data demonstrate that, as was previously shown,[21] L51P causes an increase in the effects of BMP2 on bone formation in *sham*-operated animals, leading to an increase in bone volume at the defect sites 16 weeks post-implantation compared to animals with implants loaded with 1 μg BMP only or unloaded controls. L51P alone, at 10 μg, did not induce any detectable formation of bone. In animals treated with ALN, bone formation was induced in defects filled with cylinders loaded with 10 μg BMP2 and with 1 μg BMP2/10 μg L51P, respectively.

One common feature observed in vehicle-treated control animals, which received implants loaded with either 10 μg BMP2 or 1 μg BMP2/10 μg L51P, is the presence of intact βTCP ceramic material surrounding the newly formed bone in a ring-like structure. Since the diameter of the βTCP implants exceeds the diameter of the femoral diaphysis, we hypothesized that with the present experimental setup, bone formation is constrained to a volume similar to the original bone volume. It would be of particular interest to investigate whether the remaining implant will be filled with bone and remodelled or removed without additional bone formation, if the period allowed for repair is prolonged.

Compared to the newly formed bone in the critical-size defects from control animals, bone formation in animals receiving both ALN and 10 μg BMP2 or 10 μg L51P/1 μg BMP2 exceeded the original bone volume and the

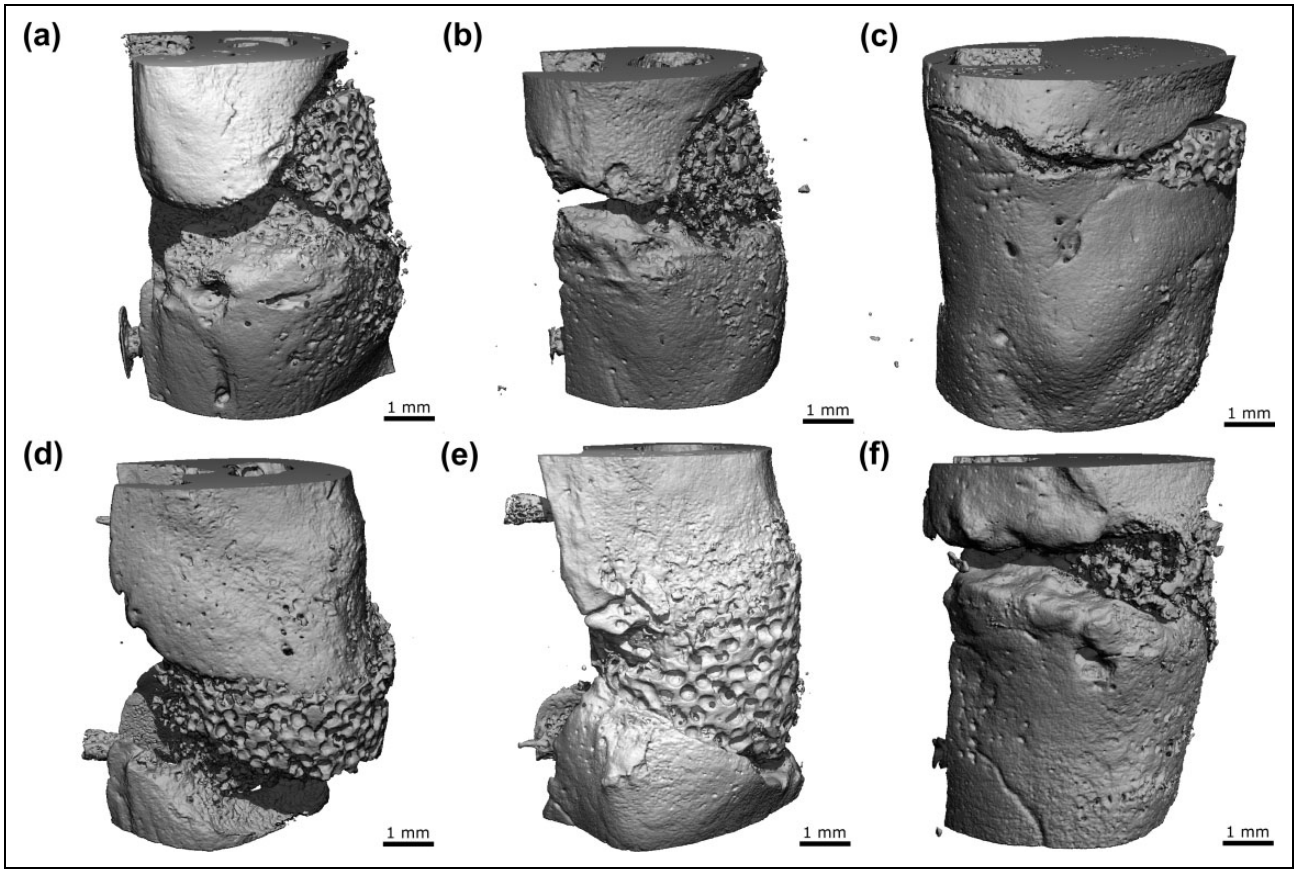

Figure 6. MicroCT 3D renderings of femoral defects. Representative renderings from critical-size femoral defects filled with cylinders loaded with 10 μg BMP2 are depicted for (a) *sham*, (b) *OVX* and (c) *OVX*/ALN. Renderings from defects filled with ceramics loaded with 1 μg BMP2/10 μg L51P are shown in panels (d) *sham*, (e) *OVX* and (f) *OVX*/ALN. Bone formation occurs preferentially at the proximal and distal ends of the implants in *sham* and *OVX* control animals irrespective of BMP2 and BMP2/L51P loading of the implants (a, b, d, e). In animals treated with ALN, bone formed from both the distal and proximal ends of the defects, the newly formed bone bridging the defect irrespective of BMP2 and BMP2/L51P loading of the implants (c, f). ALN: alendronate; *OVX*: ovariectomized; BMP: bone morphogenetic protein; microCT: micro-computer tomography.

perimeter of the implant. Besides the excessive bone formation, implant turnover was greatly reduced in animals treated with ALN. Quantitative evaluation of the remaining βTCP ceramics revealed that the volume of βTCP in ALN-treated animals was doubled when compared with the volume of βTCP in vehicle-treated animals upon loading of the ceramics with 10 μg BMP2 and 10 μg L51P/1 μg BMP2, respectively. As reported previously, bone formation and growth into the porous βTCP implants are prerequisites for the turnover of the ceramics. The inhibition of osteoclastic bone resorption by ALN, however, decreased the dissolution of βTCP ceramics, demonstrating the implant turnover to depend on osteoclast activity and not on the ceramic's chemical solubility.

In physiological bone remodelling, coupling of osteoclast and osteoblast activities is crucial for the maintenance of mass and structure of bone. In the presence of supraphysiological levels of BMP2, bone formation and resorption are uncoupled. As a consequence, in our study, bone formation induced by BMP2 was not affected in animals treated with ALN, despite the block of resorption. When animals are treated with ALN, irrespective of BMP2 levels, bone remodelling will not take place and therefore primary woven bone will not be replaced by secondary, mechanically more competent lamellar bone.

The present study provided evidence on two crucial aspects relevant to reconstructive orthopaedic surgery. Firstly, it corroborated the usefulness of the strategy to block endogenous BMP antagonists to improve the bioefficacy of exogenously added BMP. Secondly, it demonstrated the necessity for functional cellular resorption for the removal of βTCP ceramics from a repair site. There are, however, also limitations of the present model. The duration of the study was too short for a complete removal of the βTCP biomaterial. Furthermore, no biomechanical testing of the partially or fully healed defects could be performed. Despite these limitations, however, the data suggest that in patients treated with BP, healing of βTCP-filled bone defect may be impaired because of the failure to

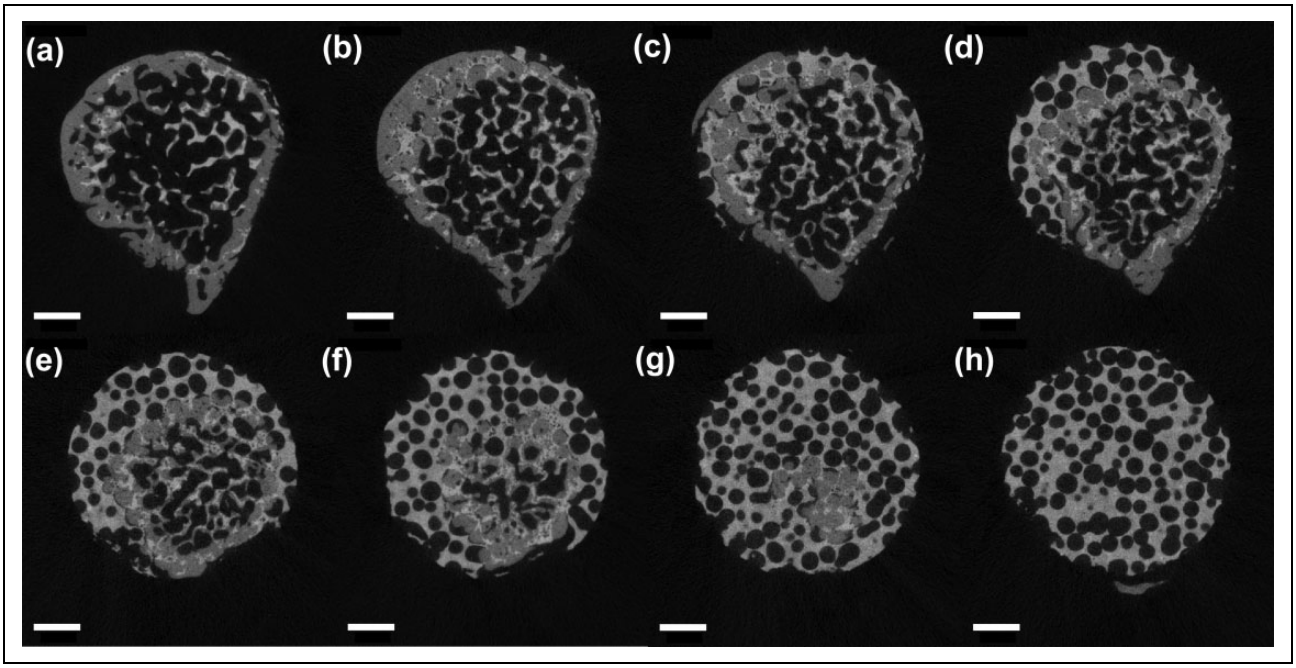

Figure 7. Two-dimensional renderings of microCT sections of ceramics and bone at the defect site. A representative panel of 2D cross-sectional microCT images, the plane of section moving in steps of 400 μm from the proximal ends of the defect towards the centre of the βTCP implant, is depicted in panels a to h. The cross-sectional area of the bone covers the entire implant surface at the distal/proximal part of the defect (a), and the bone surface decreases continuously (b–g) towards the centre of the defect (h). The images are from microCT measurements of an *OVX* control animal with βTCP implant loaded with 1 μg BMP2/10 μg L51P. Bars represent 1 mm. βTCP: β-tricalcium phosphate; BMP: bone morphogenetic protein; microCT: micro-computer tomography; *OVX*: ovariectomized.

remove the implant material and its replacement by authentic bone.

Authors' note

All authors have read and approved of the final manuscript.

Acknowledgements

The authors would like to thank Editage (www.editage.com) for English language editing.

Author contributions

Michel Hauser (Design, Experiment, Collection of Data, Interpretation, Manuscript Preparation); Mark Siegrist (Design, Experiment, Collection of Data); Alain Denzer, Nikola Saulacic and Joël Grosjean (Experiment, Collection of Data); Marc Bohner (Design, Interpretation); and Willy Hofstetter (Design, Collection of Data, Interpretation, Manuscript Preparation).

Declaration of conflicting interests

The author(s) declared no potential conflicts of interest with respect to the research, authorship, and/or publication of this article.

Funding

The author(s) disclosed receipt of the following financial support for the research, authorship, and/or publication of this article: This work was made possible by a grant from the Alfred & Anneliese Sutter-Stöttner Foundation to Willy Hofstetter.

Supplemental material

Supplemental material for this article is available online.

References

1. Johnell O and Kanis J. An estimate of the worldwide prevalence and disability associated with osteoporotic fractures. *Osteoporos Int* 2006; 17(12): 1726–1733.
2. Luckman SP, Hughes DE, Coxon FP, et al. Nitrogen-containing bisphosphonates inhibit the mevalonate pathway and prevent post-translational prenylation of GTP-binding proteins, including Ras. *J Bone Miner Res* 1998; 13(4): 581–589.
3. Rodan GA and Fleisch HA. Bisphosphonates: mechanisms of action. *J Clin Invest* 1996; 97(12): 2692–2696.
4. Black DM, Cummings SR, Karpf DB, et al. Randomised trial of effect of alendronate on risk of fracture in women with existing vertebral fractures. *Lancet* 1996; 348(9041): 1535–1541.
5. Bone HG, Downs JRW, Tucci JR, et al. Dose-response relationships for alendronate treatment in osteoporotic elderly women. *J Clin Endocrinol Metab* 1997; 82(1): 265–274.
6. Chesnut CH, McClung MR, Ensrud KE, et al. Alendronate treatment of the postmenopausal osteoporotic woman: effect of multiple dosages on bone mass and bone remodeling. *Am J Med* 1995; 99(2): 144–152.

7. Cranney A, Wells G, Willan A, et al. II. Meta-analysis of alendronate for the treatment of postmenopausal women. *Endocr Rev* 2002; 23(4): 508–516.
8. Hosking D, Chilvers CED, Christiansen C, et al. Prevention of bone loss with alendronate in postmenopausal women under 60 years of age. *N Eng J Med* 1998; 338(8): 485–492.
9. Liberman UA, Weiss SR, Bröll J, et al. Effect of oral alendronate on bone mineral density and the incidence of fractures in postmenopausal osteoporosis. *N Eng J Med* 1995; 333(22): 1437–1444.
10. Fu LJ, Tang TT, Hao YQ, et al. Long-term effects of alendronate on fracture healing and bone remodeling of femoral shaft in ovariectomized rats. *Acta Pharmacol Sin* 2013; 34(3): 387–392.
11. Gerstenfeld LC, Sacks DJ, Pelis M, et al. Comparison of effects of the bisphosphonate alendronate versus the RANKL inhibitor denosumab on murine fracture healing. *J Bone Miner Res* 2009; 24(2): 196–208.
12. Cao Y, Mori S, Mashiba T, et al. Raloxifene, estrogen, and alendronate affect the processes of fracture repair differently in ovariectomized rats. *J Bone Miner Res* 2002; 17(12): 2237–2246.
13. Urist MR, Mikulski A and Lietze A. Solubilized and insolubilized bone morphogenetic protein. *Proc Natl Acad Sci U S A* 1979; 76(4): 1828–1832.
14. Canalis E, Economides AN and Gazzerro E. Bone morphogenetic proteins, their antagonists, and the skeleton. *Endocr Rev* 2003; 24(2): 218–235.
15. Walsh DW, Godson C, Brazil DP, et al. Extracellular BMP-antagonist regulation in development and disease: tied up in knots. *Trends Cell Biology* 2010; 20(5): 244–256.
16. Dean DB, Watson JT, Jin W, et al. Distinct functionalities of bone morphogenetic protein antagonists during fracture healing in mice. *J Anatomy* 2010; 216(5): 625–630.
17. Haque T, Hamade F, Alam N, et al. Characterizing the BMP pathway in a wild type mouse model of distraction osteogenesis. *Bone* 2008; 42(6): 1144–1153.
18. Kloen P, Doty SB, Gordon E, et al. Expression and activation of the BMP-signaling components in human fracture nonunions. *JBJS* 2002; 84(11): 1909–1918.
19. Keller S, Nickel J, Zhang JL, et al. Molecular recognition of BMP-2 and BMP receptor IA. *Nat Struct Mol Biol* 2004; 11(5): 481–488.
20. Albers CE, Hofstetter W, Sebald H-J, et al. L51P – a BMP2 variant with osteoinductive activity via inhibition of Noggin. *Bone* 2012; 51(3): 401–406.
21. Sebald HJ, Klenke FM, Siegrist M, et al. Inhibition of endogenous antagonists with an engineered BMP-2 variant increases BMP-2 efficacy in rat femoral defect healing. *Acta Biomaterialia* 2012; 8(10): 3816–3820.
22. Khattab HM, Ono M, Sonoyama W, et al. The BMP2 antagonist inhibitor L51P enhances the osteogenic potential of BMP2 by simultaneous and delayed synergism. *Bone* 2014; 69: 165–173.
23. Khattab HM, Kubota S, Takigawa M, et al. The BMP-2 mutant L51P: a BMP receptor IA binding-deficient inhibitor of noggin. *J Bone Miner Metab* 2018; 1: 1–7.
24. Sato M, Grasser W, Endo N, et al. Bisphosphonate action. Alendronate localization in rat bone and effects on osteoclast ultrastructure. *J Clinical Investigation* 1991; 88(6): 2095–2105.
25. Kirsch T, Nickel J and Sebald W. Isolation of recombinant BMP receptor IA ectodomain and its 2 :1 complex with BMP-2. *FEBS Lett* 2000; 468(2-3): 215–219.
26. Ruppert R, Hoffmann E and Sebald W. Human bone morphogenetic protein 2 contains a heparin-binding site which modifies its biological activity. *Eur J Biochem* 1996; 237(1): 295–302.
27. Gröngröft I, Heil P, Matthys R, et al. Fixation compliance in a mouse osteotomy model induces two different processes of bone healing but does not lead to delayed union. *J Biomech* 2009; 42(13): 2089–2096.
28. Bouxsein ML, Boyd SK, Christiansen BA, et al. Guidelines for assessment of bone microstructure in rodents using micro–computed tomography. *J Bone Miner Res* 2010; 25(7): 1468–1486.
29. Wernike E, Montjovent MO, Liu Y, et al. VEGF incorporated into calcium phosphate ceramics promotes vascularisation and bone formation in vivo. *Eur Cell Mater* 2010; 19: 30–40.
30. MacNeal WJ. Tetrachrome blood stain: an economical and satisfactory imitation of Leishman's stain. *JAMA* 1922; 78: 122–121.
31. Penney D, Powers J, Frank M, et al. Analysis and testing of biological stains – the biological stain commission procedures. *Biotech Histochem* 2002; 77(5–6): 237–275.
32. Arganda-Carreras I, Kaynig V, Schindelin J, et al. Trainable WEKA segmentation: a machine learning tool for microscopy image segmentation. *Neuroscience* 2014; 34(15): 73–80.
33. McClung M, Harris ST, Miller PD, et al. Bisphosphonate therapy for osteoporosis: benefits, risks, and drug holiday. *Am J Med* 2013; 126(1): 13–20.